INITIAL INVESTIGATION OF SELECTIVE LASER SINTERING LASER POWER VS. PART POROSITY USING IN-SITU OPTICAL COHERENCE TOMOGRAPHY

Adam Lewis[1], Austin McElroy[2], Thomas Milner[2], Scott Fish[3], Joseph Beaman[3]

[1]McKetta Department of Chemical Engineering
[2]Department of Biomedical Engineering
[3]Department of Mechanical Engineering
Cockrell School of Engineering, The University of Texas at Austin, Austin, TX 78705

Abstract

Additional types of process sensors could be useful in further improving consistency of Selectively Laser Sintered (SLS) parts. Optical Coherence Tomography (OCT) has shown promise as a new SLS process sensor which can yield depth resolved data not attainable with conventional sensors. This study investigates the use of OCT as a tool to determine part porosity. Various laser powers were used during the build and the in-situ OCT data corresponding to the various laser powers are compared. The finished part was then imaged using X-ray Computed Tomography (XCT). Porosity data was obtained and is compared with the OCT data.

Introduction

Selective Laser Sintering

Selective Laser Sintering (SLS) is a powder bed fusion process developed at UT Austin in the late 1980's and early 1990's. It was one the first commercialized additive manufacturing technologies. SLS continues to be relevant as an additive technique in various industries including aviation and the 3D printed medical devices market among others in part due to its ability to produce parts comparable to those created by injection-molding. A schematic demonstrating how the SLS process works is shown in Figure 1 from Gibson et al [1].

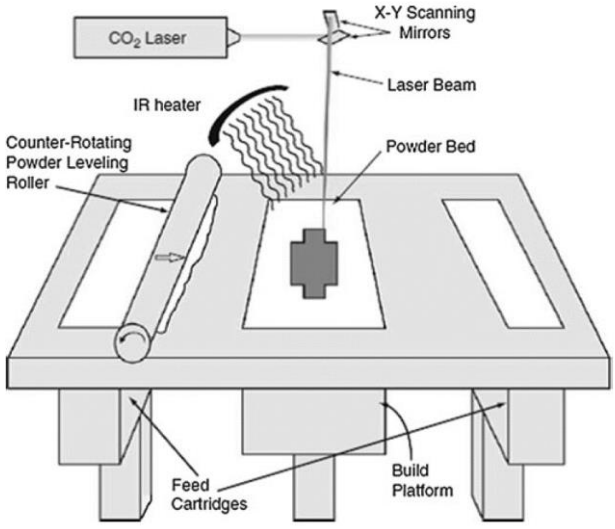

Figure 1. Selective Laser Sintering Schematic [1]

During the build process, the roller will spread a thin (often 200 μm or less) layer of semicrystalline polymer powder on the powder bed. The powder is then heated to within about 10°C of its melting point by an IR heater. Next, a laser beam directed by a set of scanning mirror galvanometers is used sinter a cross section of the part being built. After sintering, a new layer of powder is spread and heated and the next cross sectional layer of the part is sintered to itself as well as the layer below. These steps are repeated many times until the part is completely built. Finally, the part is cooled slowly in order to prevent large thermal stresses from accumulating and causing warpage in the part.

Despite the applications of SLS in various industries, it is common for SLS part properties to vary, even amongst different specimen contained within the same build. A desire to improve consistency of parts has led to an interest in improved process sensing and control in the SLS process. One of the technologies being investigated as an improved process sensor for SLS is Optical Coherence Tomography (OCT).

Optical Coherence Tomography

Optical coherence tomography (OCT) is an established medical imaging technique based on coherence interferometry commonly used in biomedical optics and medicine. In that application, OCT has the ability to provide real time subsurface visualization of human tissues at sub 10μm resolution. OCT data can be used to produce cross-sectional and volumetric images from magnitude and echo time delay data of backscattered radiation. A single OCT scan at a point on the surface of the sample is known as an A-scan and yields depth information at this point. A collection of subsequent A-scans is called a B-scan and yields a cross sectional image of the sample. Subsequent B-scans can be combined to yield a 3D representation of the sample as shown in Figure 2. The backscattered intensity information is typically presented in the false color of B-scans and volumetric renderings.

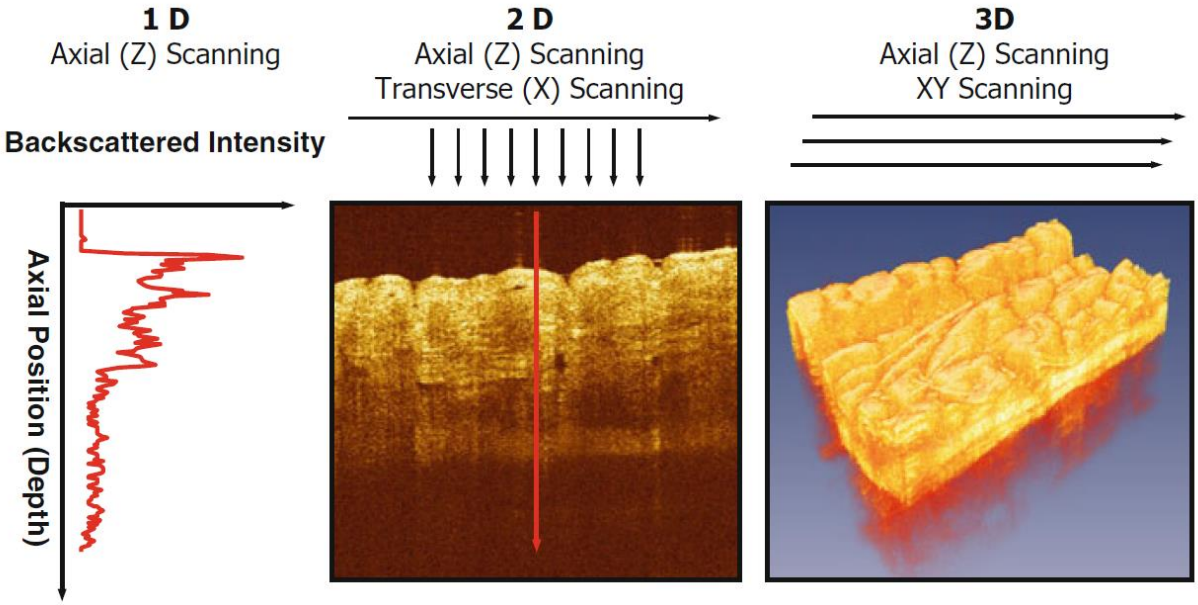

Figure 2. Typical OCT data visualization (Left) A-scan (Middle) B-scan (Right) Volumetric Rendering [2]

Optical Coherence Tomography in Selective Laser Sintering

Research applying OCT to SLS is sparse. Some work has been done analyzing surface voids, surface roughness and subsurface unsintered powder after parts have been built [3], [4]. In-situ use of OCT has also been explored. In 2016, Lewis et al. boresighted an OCT imaging laser with the sintering laser on an SLS machine in order to image during the SLS build process [5]. Initial images seemed promising, showing that multiple layers could be imaged simultaneously and also allowing part curl to be identified before it caused a build to fail. The present work builds on the initial work by Lewis et al. in further investigating the usefulness of OCT as a process sensor in SLS. Various researchers have shown a strong correlation between part density and strength in SLS parts [6], [7]; therefore, correlations of OCT data to local part density & porosity will be given special attention here.

Materials and Methods

Nylon Powder

All of the powder imaged in this paper was commercially available, virgin PA650 (nylon 12) from Advanced Laser Materials (ALM). The data sheet provided by ALM gives a particle size range, D10-D90, of 30 to 100 μm and a mean particle diameter of 55 μm. The melting temperature is reported at 181°C.

LAMPS Machine & OCT System

The in-situ OCT imaging was performed via an OCT system installed on the Laser Additive Manufacturing Pilot System (LAMPS) machine. The LAMPS machine was designed and built at The University of Texas at Austin as a research SLS printer capable of increased measurement and control of process variables. The LAMPS machine features visual and infrared cameras as well as approximately 40 strip heaters and associated thermocouples for precise control of the chamber, build box, and powder surface temperatures. A more complete description of the LAMPS System can be found in Wroe et al. [8] and Fish et al. [9]. Figure 3 shows the LAMPS machine as well as a cross section of the build chamber [5]. Typical parts are built using a two-thirds beam overlap and 45% laser power.

The OCT laser was boresighted with the CO_2 sintering laser as described in Lewis et al. [5] and had the specifications given in Table 1.

Table 1: OCT System Specifications

Swept Source Laser Parameters			
Average Output Power	30 mW	Sweep Rate	100 kHz
Central Wavelength	1310 nm	Wavelength Tuning Range	140 nm
Resolution Parameters			
Axial Spatial Resolution	Not Measured	Lateral Spatial Resolution	186 μm
Axial Pixel Resolution	4.76 μm/pixel	Lateral Pixel Resolution	15 μm/pixel

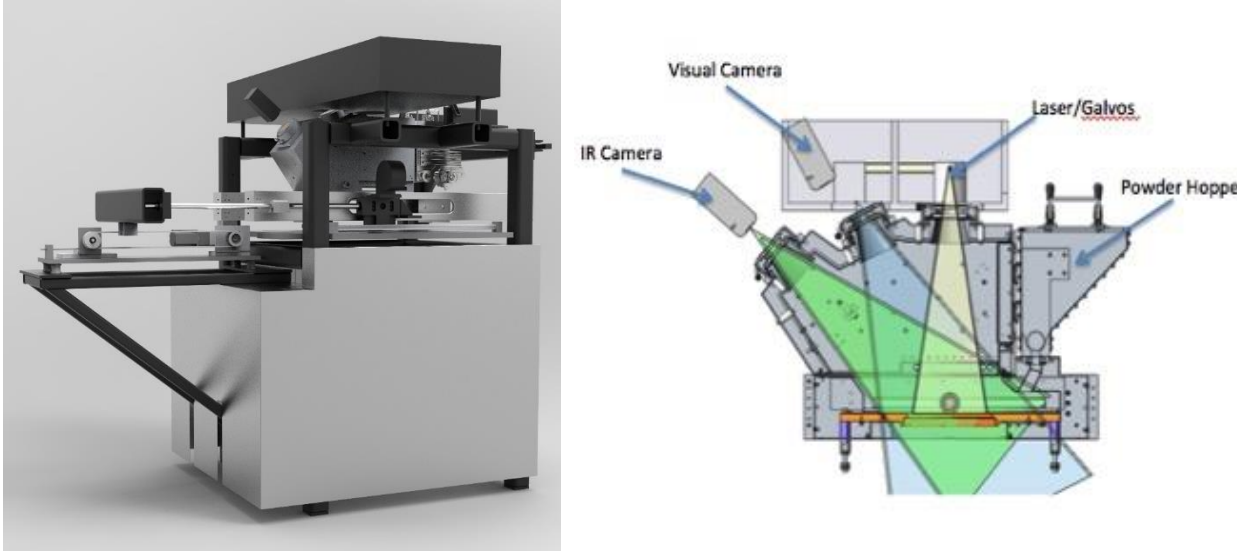

Figure 3 – (Left) External View of LAMPS CAD geometry (Right) LAMPS Build Chamber Cross Section [5]

XCT System

The CT data was collected using a microXCT 400 scanner built by Zeiss using a 4X objective, 70kV, 143 µA and 1261 projections. The data was reconstructed into 16 bit TIFF images by Xradia Reconstructor producing data divided into cubic voxels with each side being 5.54 µm in length. Subsequent image processing and analysis was performed using FIJI, a distribution of ImageJ [10].

SLS Part and Scan Strategy

A 49 layer cylinder with a diameter of approximately 5.5 mm was built. The laser power was increased periodically as listed in Table 2. Although the OCT and CO_2 laser used the same set of galvos, the beams focused at different locations on the powder surface. This necessitated separate sintering and imaging time periods using the galvos as opposed to concurrent imaging/sintering. Concurrent imaging/sintering would likely not yield a good view of the melt pool because the powder would not have time to melt by the time the galvos have moved on, directing the beam to another spot on the powder.

Table 2: Part Layer Number vs Sintering Laser Power

Layer Number	Laser Power
1-9	20.0%
10-19	32.5%
20-29	45.0%
30-39	57.5%
40-49	70.0%

The sintering/imaging sequence was as follows for each build layer:

1. An 11.5 mm square shape was sintered around the cylinder area for image alignment in post processing
2. Two pre-sintering imaging scans were taken of the area to be sintered using scan spacing identical to the scan spacing during sintering (0.2794 mm).
3. The cylinder was sintered by scan lines with a two-thirds beam overlap.
4. Two post-sintering imaging scans of the area around the sintered cylinder cross-section were taken.
5. The outline of the cylinder was re-sintered.

The cylinder sintering scan lines directions alternated such that all odd layers were sintered with scan lines perpendicular to the imaging scan lines while the even layers were sintered with scan lines parallel with the imaging scan lines.

Initial Post Processing of Data

OCT imaging was started through a manual trigger with the start of sintering of each layer and continued for roughly 20 seconds. A bug in the OCT collection software caused the OCT data to be corrupted/unusable for several of the build layers. For all of the data which was collected normally, the following background subtraction technique was applied. Previously, 512 A-scans were collected with nothing in the sample arm and averaged together. This average A-scan was subtracted from each A-scan in the rest of the data to remove background noise and give a higher signal to noise ratio (SNR).

Each layer's 20 seconds of OCT data resulted in a data file over 4 GB in size consisting of approximately 2 million A-scans of data. Each layer's data had to be "cut" into ninety-six meaningful, smaller B-scans per layer corresponding to the imaging scan lines in order to be analyzed effectively.

Results & Discussion

OCT Data

A number of observations could be made immediately after the initial post processing. The 20% power layers had almost no noticeable meltpool in the OCT images while the higher laser powers had a more transparent, visible meltpool present as shown in Figure 4 (a) & (b). Additionally, it could be seen that the meltpool was generally deeper on the outline of the part where the part outline scan had been as seen in Figure 4 (a)-(f). As mentioned in the SLS Part and Scan Strategy section, two post-scans were performed for each layer. The bottom and the surface of the meltpool were generally more visible in the second post scan than the first as shown in Figure 4 (c) & (d). This could possibly be because the surface had cooled slightly more and solidified more in the second post scan than it had in the first post scan. Multiple layers could be seen at time at certain layers as shown in Figure 4 (e). Small, brightly reflecting objects could also be seen in the OCT data as shown in Figure 4 (f). These may be pores or perhaps some contaminant in the powder.

The meltpool depth vs. layer number was then examined. To do this, each of the twenty-four b-scans corresponding to the second post OCT scan in each layer were analyzed in the

following manner. One hundred A-scans in the middle of the meltpool were averaged together. The averaged A-scan was then put through a moving average filter with a window length of 15 twice consecutively in order to further improve the SNR. Then, starting from the bottom of the image, The first point above a certain threshold was found and defined as the meltpool depth. This process is illustrated in Figure 5.

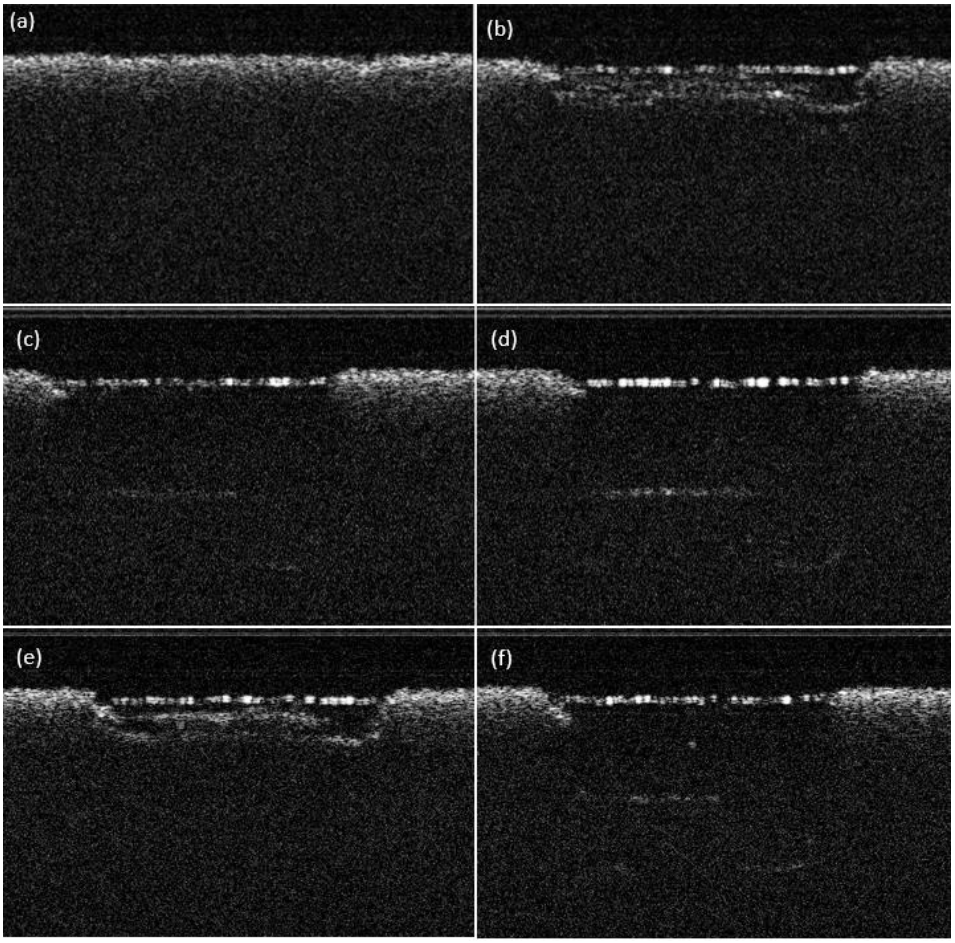

Figure 4 (a) Layer 3, Laser Power: 20%, B-scan: 38, Post 2 (b) Layer 28, Laser Power: 45.0%, B-scan: 38, Post 2 (c)&(d) Layer 43, Laser Power: 70%, B-scan 33, Post 1 (left) and Post 2 (right) (e) Layer 27, Laser Power 45%, B-scan 33, Post 2, (f) Layer 42, Laser Power: 70%, B-scan: 32, Post 1

These results are summarized in Figure 6. The 24 b-scans of interest for each layer are in the columns and the layers are given by the rows. The laser power used on each layer is noted on the right hand side. Rows for which data wasn't collected properly are shaded red. The leftmost and rightmost b-scans were scan lines before and after the item so the depth detected by them is relatively constant. Additionally, the first 12 layers are grayed out because not much of a meltpool had formed at this point so the meltpool detection algorithm results should be viewed cautiously here. The b-scans of the edges of the meltpool (28-31, 46-47) appear to be slightly deeper than in the center of the meltpool starting at about layer 31. This is consistent with the earlier observation that the outline of the part had a deeper meltpool than the center.

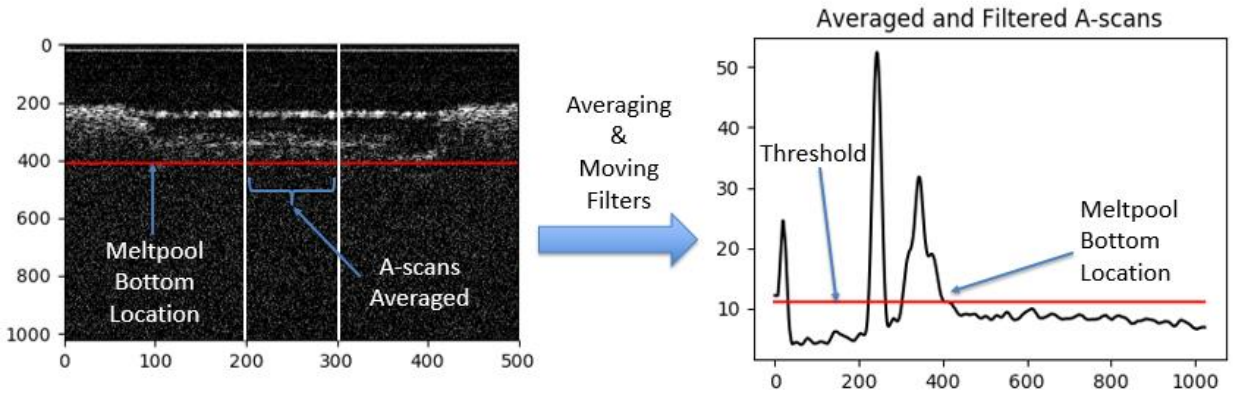

Figure 5. 100 A-scans (between vertical white lines) were averaged and filtered and then the last location above a certain threshold was defined to be the meltpool bottom.

The median of the meltpool bottom locations of each layer was recorded and graphed vs. layer number in Figure 7. Starting at layer 16, there is a positive, linear growth to the layer number. The growth is dramatically decreased at layers 24 and 32, but otherwise the linear trend increases. The slope of the line of best fit from layer 16-22 is only 19.3 pixels/layer, but the slope of the lines of best fit from 24-31, and 32-49 are both around 27 pixels/layer. After viewing the data, it is apparent that the meltpool being viewed in each of the last two line segments is the same layer and the 27 pixel increase corresponds to a new melted layer thickness. It is thought that the meltpool depth drops dramatically when the top sintered layer is either not fully sintered or when it cools and begins to recrystallize before the next layer of powder is spread on top. This causes the layer to be highly scattering and the visibility of the layers beneath the highly scattering layer to be greatly reduced. The highly scattering layer number can be approximated by examining how many layers (~27 pixels) beneath the current layer is the highly scattering layer. In this case, it was determined that the highly scattering layers were layers 23 and 31. Although it is not yet clear what effect these highly scattering layers have on the final part, it may be possible to re-sinter a region to eliminate the highly scattering layer imaging obstacle. On the layers where multiple layers were visible, the distance between peaks could be used to estimate layer thickness though this has not been done in the present analysis.

The vertical location of the surface of the powder/meltpool before and after sintering was also determined by averaging 100 A-scans in the middle of the same b-scan on each layer. The results are shown in Figure 8 and Figure 9. It can be seen there is a periodic oscillation in the height of both the surface of the powder and meltpool. The period is approximately 8 layers. This oscillation could be due to eccentricity in the roller which would be effectively mean some layers are thicker than others. Given that both the nominal layer thickness and the peak to trough distance are roughly 100 microns, some layers may be twice as thick as other layers. This is problematic because the bottom portions of a thicker layer may not be fully sintered by a laser power which will sinter the thinner layers without a problem. The fact that the two highly scattering layers, 23 & 31, roughly correspond to peaks in Figure 8 and are 8 layers apart lends additional evidence to the thicker layer hypothesis. It is possible that the higher laser powers

were sufficient to sinter through even the thicker layers which would explain why the highly scattering layers didn't occur after layer 31.

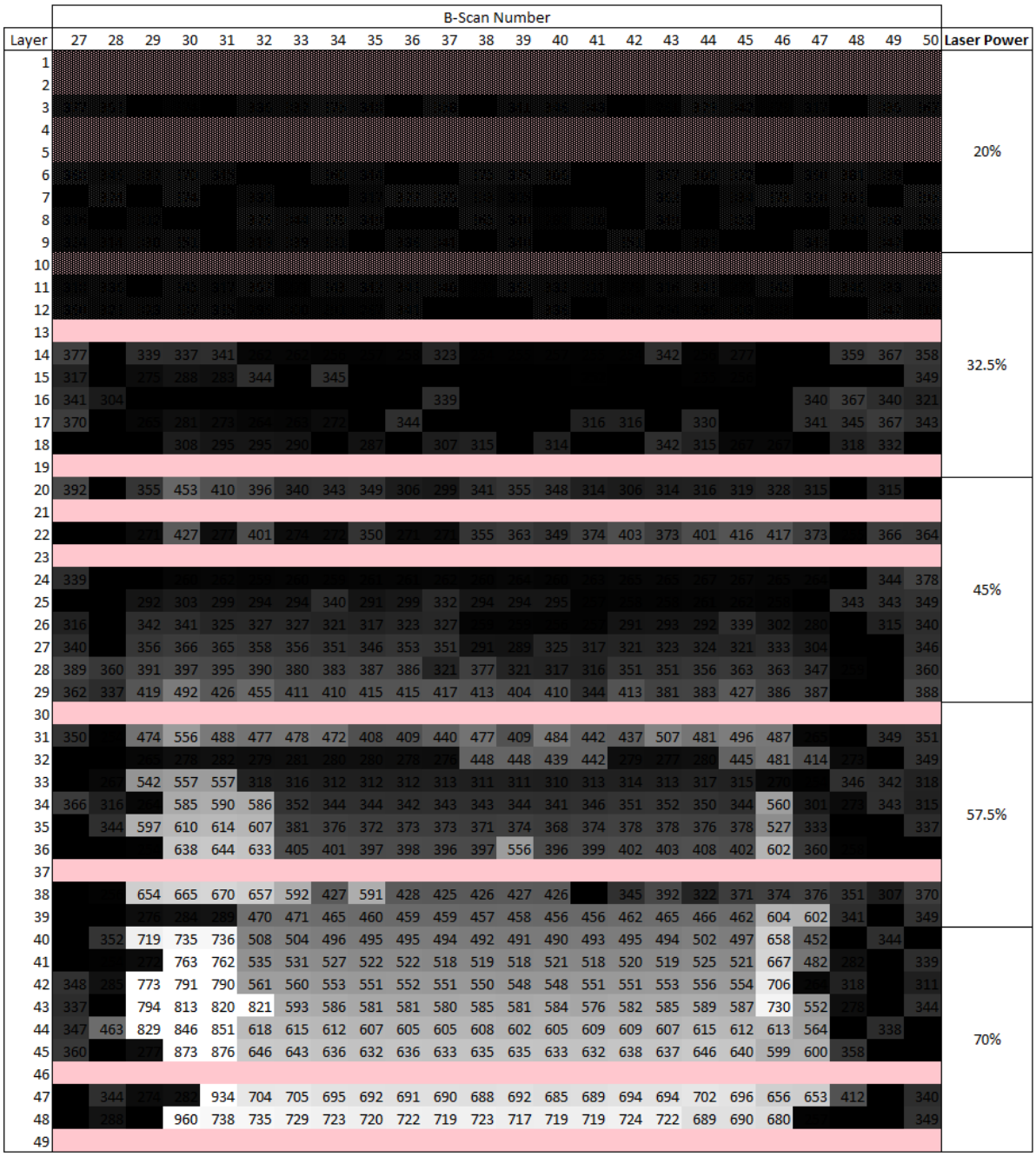

Figure 6. Meltpool bottom location of each b-scan on each layer

Figure 9 shows the difference in the top surface of powder or meltpool and is hereafter referred to as the "layer fall." The layer fall does generally increase over the layers although the coefficient of determination is only 0.54. The layer fall may increase due to the higher laser powers more fully melt the powder or as the higher laser powers vaporize some of the polymer or cause additional material ejection.

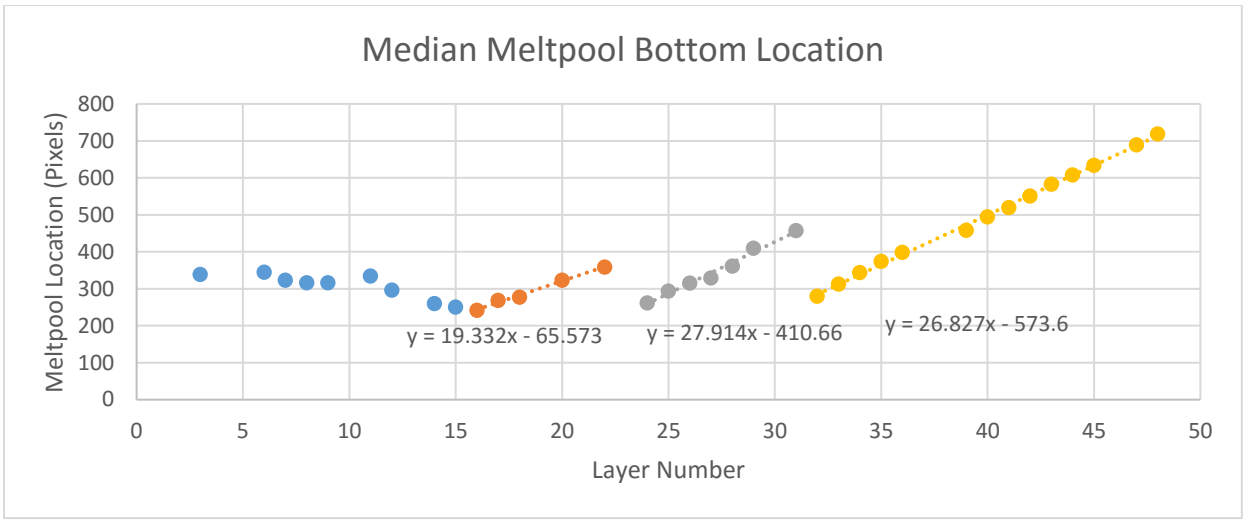

Figure 7. Median Meltpool Bottom Location vs. Layer Number

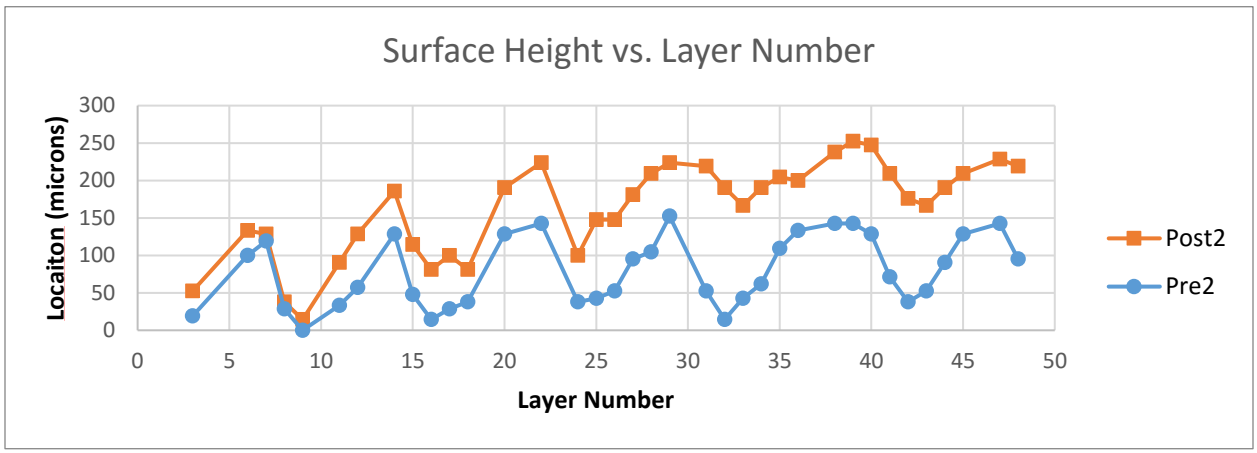

Figure 8. Powder/Meltpool Height vs. Layer Number

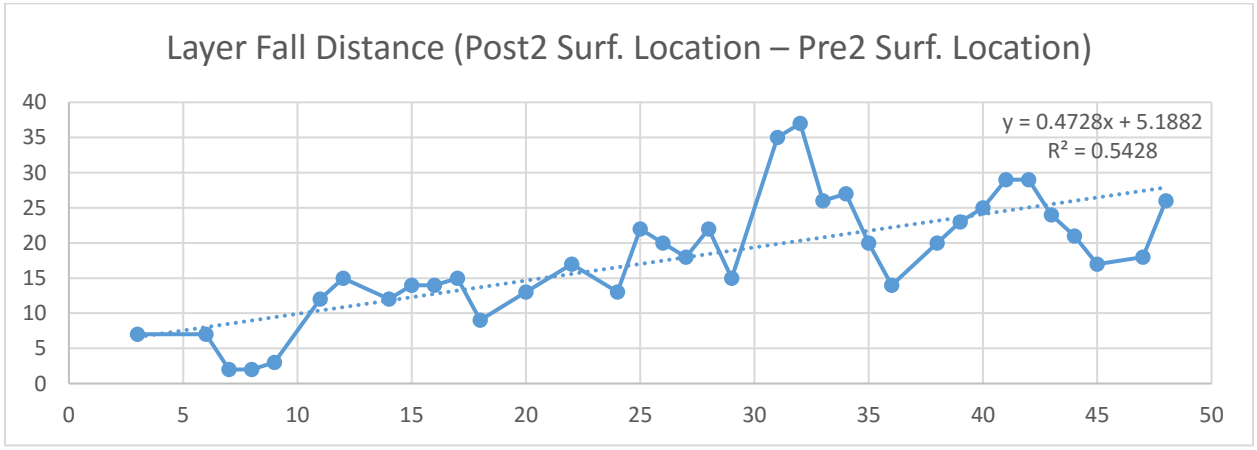

Figure 9. Layer Fall Distance vs. Layer Number

XCT Data

The 49 layer cylinder was imaged with XCT after being built. The cylinder diameter was slightly larger than the 5.5mm field of view of the XCT images so a small portion of the cylinder was not able to be imaged, but the majority of the cylinder was. Additionally, the layers printed at lower laser powers had a slightly smaller diameter than those printed at higher laser powers due to additional part growth.

Initially, the XCT images were rotated in FIJI [10] to better align with the layers visible in the XCT data. The density was then approximated by selecting a region of interest (ROI) which was part of the cylinder through the entire image stack (since the layers sintered at lower laser powers were smaller in area than the layers sintered at higher laser powers). The number of pixels above a certain threshold in the ROI divided by the total number of pixels in the ROI gave an approximation of the porosity of each XCT layer. The resulting density is shown in Figure 10 with Figure 11 and Figure 12 showing zoomed in regions of Figure 10.

Oscillations in density can be seen in some portions of the XCT data, as also seen in previous literature [11], but not in others. In the region where oscillations are found, the peaks are spread about 14-16 pixels apart which correspond to layer thicknesses of around 78-89 microns in the cooled part. It is difficult to differentiate exactly which layers were sintered with higher laser powers based on the XCT data. Given the part growth which is occurring at the higher laser powers, it is also difficult to tell precisely where the sintered material ends and the part growth begins at layers 800 and above.

Several other observations were made. The earlier layers sintered at lower laser powers appeared more as loosely sintered powder particles compared to the layers sintered at higher laser powers as shown in Figure 13 and Figure 14. Portions of the outline of Figure 13 also seem to have been sintered more fully likely as the outline scan deposited more energy on those parts. Additionally, either pores or some highly scattering foreign material were also visible in the XCT images as pointed out in Figure 14.

Correlations to Porosity

Several of the OCT results shown are promising correlations to local part porosity. The fact that peaks from multiple, subsequent layers can be seen in a single B-scan and the fact that the powder surface location can be measured so precisely may both provide ways to measure each layer's thickness. As noted earlier, thicker layers are more likely to be less sintered towards the bottom, increasing porosity. Additionally, it is possible that those thicker layers are the brightly scattering layers (23 & 31) seen in this work. It is likely that sintering such layers with additional energy could more fully sinter those layers and therefore reduce porosity.

It was not clear if the highly reflecting subsurface objects in the OCT images were pores, foreign material, or something else. If they were pores, detecting them would obviously give some knowledge about the local part density since pores are less dense than sintered material. The meltpool would need to be scanned with higher resolution to confirm this. Layer fall also may also be promising, and will be considered in future experiments.

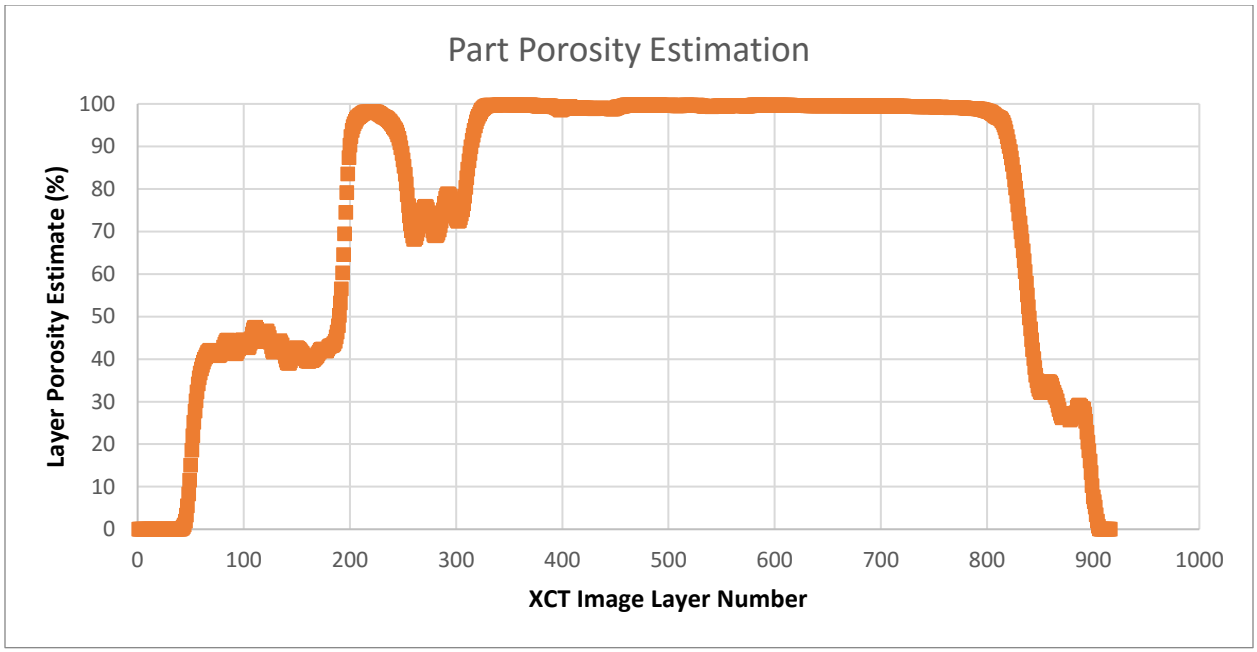

Figure 10. Porosity Estimate of Cylinder vs. XCT Layer Number

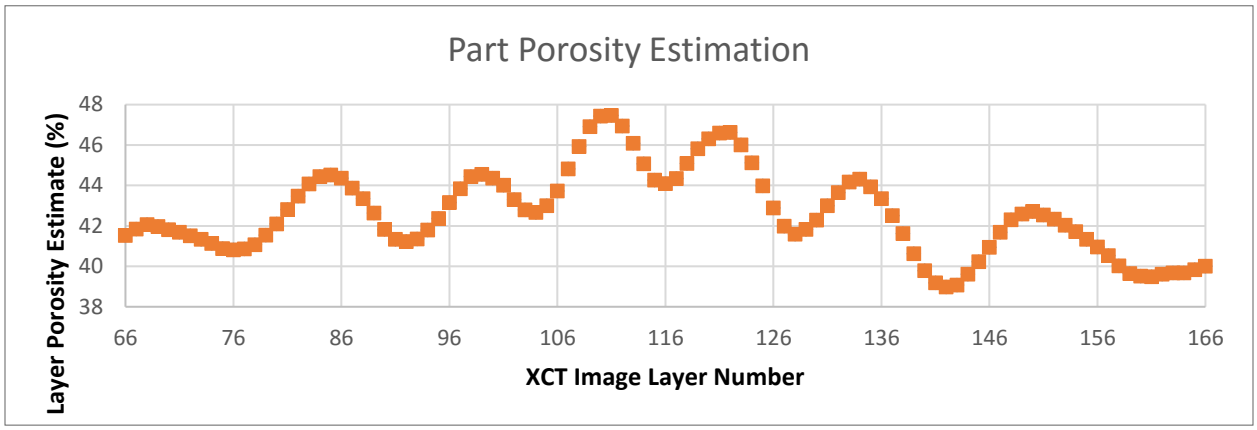

Figure 11. Zoomed in Region of Figure 10

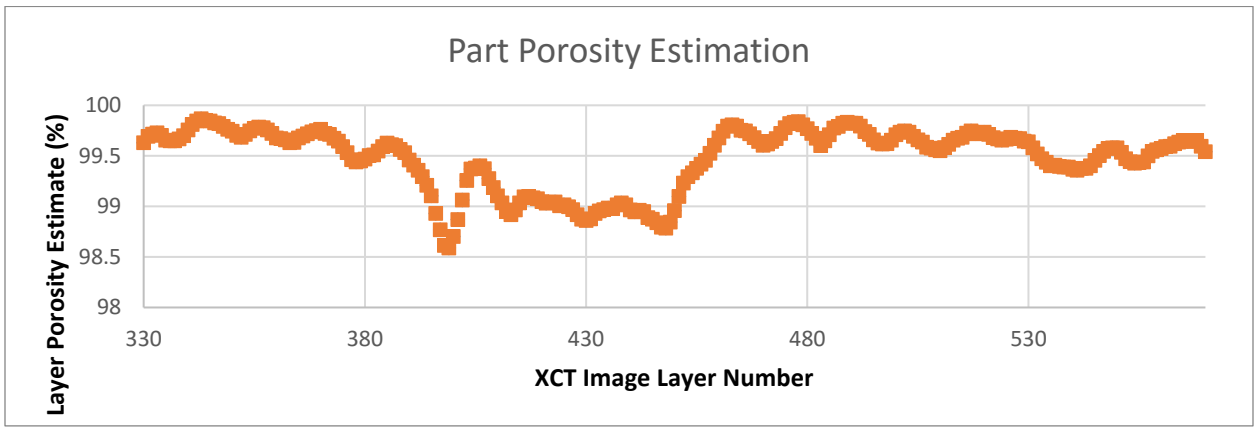

Figure 12. Zoomed in Region of Figure 10

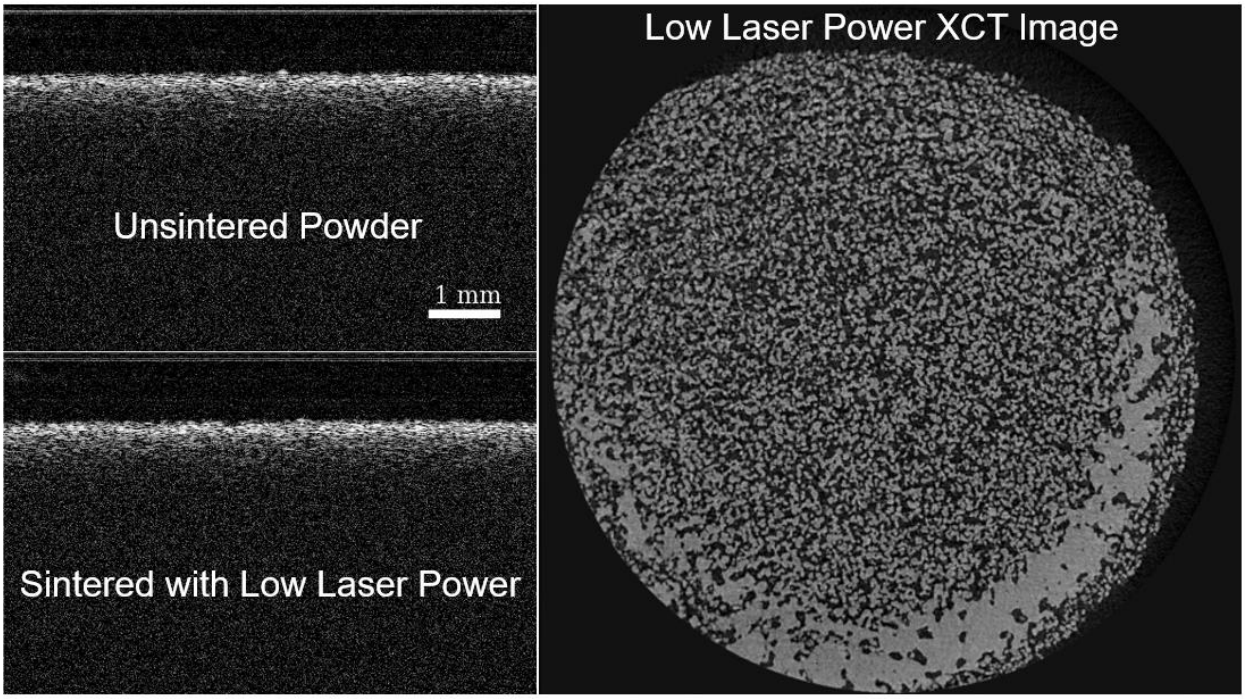

Figure 13. (Left Top) OCT Image before sintering the nylon powder. (Left Bottom) OCT Image after sintering the nylon powder at a low laser power. (Right) XCT Image of a layer sintered with low laser power.

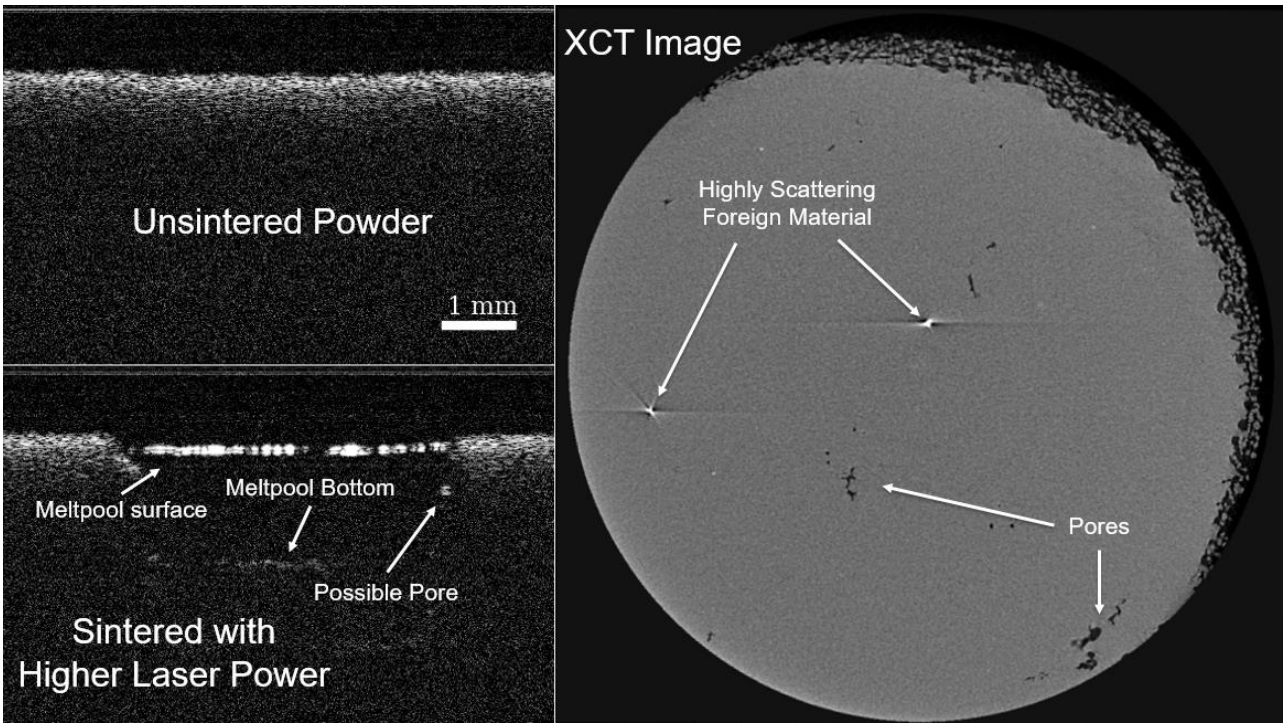

Figure 14. *(Left Top) Pre Sinter OCT Image (Left Bottom) OCT Image after melting powder. A meltpool and possibly a pore are visible. (Right) An XCT Image of the cylinder cross section is shown with pores and foreign material as indicated.*

Conclusions

In this work, a cylinder was sintered with increasing laser powers and each layer was imaged in-situ at build time with OCT. After cooling normally, the part was also imaged with XCT. Various observations were made about the OCT images and hypotheses were presented to explain them. Several of the observations show promise as methods for correlation with local part porosity though additional experimentation is still needed to confirm their usefulness. Correlations to local part porosity could be useful in new control schemes for improved SLS part consistency and quality.

Future Work

The present work will be expanded upon in a few ways. First, although highly scattering layers were identified. They were only identified after a new layer of powder had been spread and sintered on top of the highly scattering layer. It would be useful to be able to identify them before spreading a new layer of powder to improve the possibility of correcting the highly scattering layer through resintering or some other method. The relative surface brightness of the highly scattering layer to other layers seems like a promising differentiator although it has not been investigated as of the writing of this work. Additionally, although the wide range of laser powers was useful to identify overarching trends, a typical build will use only a single laser power. In order to focus on the correlations and data most relevant to typical builds, a similar experiment as the one shown here should be carried out but using a consistent laser power representative of typical builds. Additionally, although multiple layers were able to be seen in this work on some layers, using those to determine layer height has not yet been done, and should be in the future. Layer fall though mentioned here will also need to be further investigated. Finally, a good understanding of how a cooling part will appear in OCT images would also be beneficial and should be investigated moving forwards.

Acknowledgements

The authors would like to acknowledge the instrumental research support of the Air Force Research Lab (AFRL); General Dynamics Information Technology, Inc. (GDIT) PO# 08ESM753983: Laser Additive Manufacturing - Pilot Scale System (LAMPS) (PI: Scott Fish); the Office of Naval Research (ONR) Award# N00014-12-1-0811/N00014-16-1-2393: Physics and Cyber-Enabled Manufacturing Process Control for Direct Digital Manufacture of Metal Parts (PI: Joseph Beaman); and the National Science Foundation (NSF) Award # CNS-1239343: CPS: Synergy: Cyber Enabled Manufacturing Systems for Small Lot Manufacture (PI: Joseph Beaman) for their support of this research.

References

[1] I. Gibson, D. W. Rosen, and B. Stucker, *Additive Manufacturing Technologies : Rapid Prototyping to Direct Digital Manufacturing*. Boston: Springer, 2009.

[2] W. Drexler and J. G. Fujimoto, *Optical coherence tomography: technology and applications*, Second edition. Cham: SpringerReference, 2015.

[3] G. Guan *et al.*, "Evaluation of selective laser sintering processes by optical coherence tomography," *Mater. Des.*, vol. 88, pp. 837–846, Dec. 2015.

[4] G. Guan, M. Hirsch, W. P. Syam, R. K. Leach, Z. Huang, and A. T. Clare, “Loose powder detection and surface characterization in selective laser sintering via optical coherence tomography,” *Proc R Soc A*, vol. 472, no. 2191, p. 20160201, Jul. 2016.
[5] A. Lewis, M. Gardner, A. McElroy, T. Milner, S. Fish, and J. Beaman, “In-Situ Process Monitoring and Ex-Situ Part Quality Assessment of Selective Laser Sintering Using Optical Coherence Tomography,” in *Process Development*, Austin, TX, 2016.
[6] B. Caulfield, P. E. McHugh, and S. Lohfeld, “Dependence of mechanical properties of polyamide components on build parameters in the SLS process,” *J. Mater. Process. Technol.*, vol. 182, no. 1–3, pp. 477–488, Feb. 2007.
[7] H. C. H. Ho, I. Gibson, and W. L. Cheung, “Effects of energy density on morphology and properties of selective laser sintered polycarbonate,” *J. Mater. Process. Technol.*, vol. 89–90, pp. 204–210, May 1999.
[8] W. Wroe, J. Gladstone, T. Phillips, A. McElroy, S. Fish, and J. Beaman, “In-Situ Thermal Image Correlation with Mechanical Properties of Nylon-12 in SLS,” in *Materials*, Austin, TX, 2015.
[9] S. Fish, S. Kubiak, W. Wroe, J. Booth, A. Bryant, and J. Beaman, “A High Temperature Polymer Selective Laser Sintering Testbed for Controls Research,” in *Process Development*, Austin, TX, 2015.
[10] J. Schindelin, *Fiji: an open-source platform for biological-image analysis*, vol. 9(7). 2012.
[11] M. Pavan, T. Craeghs, J.-P. Kruth, and W. Dewulf, “Understanding the Laser Sintering of Poolymers at Microscale Level by using X-Ray Computed Tomography,” in *Process Development*, Austin, TX, 2016.